Niobium-added titanium oxides powders as non-noble metal cathodes for polymer electrolyte fuel cells – Electrochemical evaluation and effect of added amount of niobium

Akimitsu Ishihara[1,*], Masazumi Arao[2], Masashi Matsumoto[2], Tsubasa Tokai[3], Takaaki Nagai[3], Yoshiyuki Kuroda[3], Koichi Matsuzawa[3], Hideto Imai[2], Shigenori Mitsushima[1,3], and Ken-ichiro Ota[3]

[1] Institute of Advanced Sciences, Yokohama National University, 79-5 Tokiwadai, Hodogaya-ku, Yokohama 240-8501 JAPAN

[2] Device Analysis Department, NISSAN ARC Ltd., 1 Natsushima-cho, Yokosuka 237-0061, JAPAN

[3] Green Hydrogen Research Center, Yokohama National University, 79-5 Tokiwadai, Hodogaya-ku, Yokohama 240-8501 JAPAN

*E-Mail: ishihara-akimitsu-nh@ynu.ac.jp

Tel.: +81-45-339-4021; Fax: +81-45-339-4024.

Abstract

An appropriate evaluation of oxide-based compound powders as non-platinum cathodes for polymer electrolyte fuel cells is required to investigate the active sites of oxide-based cathodes for the oxygen reduction reaction. A mixture of carbon black powder as an electro-conductive material with oxide catalysts that had low electrical conductivity was attempted to evaluate the ORR activity. An appropriate mixture of carbon black and the oxide catalysts let to the electrochemical activation of the oxide surface by the formation of electron conduction networks. Using the carbon black mixture, the niobium-added titanium oxides heat-treated at 700 °C for 10 min under Ar containing 4% hydrogen without carbon materials were focused on to reveal the dependence of ORR activity on the added amount of niobium. The ORR activity of the niobium-added titanium oxides increased the Nb mole percentage from 0 to 20. This was due to the increase in the ratio of the $Ti^{3+}/(Ti^{4+}+Ti^{3+})$, and suggests that the active sites were Ti^{3+} and/or oxygen vacancies in the anatase phase. On the other hand, although the ratio of the $Ti^{3+}/(Ti^{4+}+Ti^{3+})$ of the oxide catalyst with an Nb mole percentage of 30 was almost twice as that with an Nb mole percentage of 20, the oxygen reduction reaction (ORR) activities were almost the same. This might be responsible for the deposition of the amorphous phase composed of Nb_2O_5, which consisted of a thin layer on the surface of the oxide particles and had low ORR activity.

Keywords: Niobium-added titanium oxides; Oxygen reduction reaction; Polymer electrolyte fuel cells; Non-platinum cathode

1. Introduction

Polymer electrolyte fuel cells (PEFCs) are expected to be one of the main power generators in the renewable hydrogen energy-based society because of their high theoretical energy efficiencies and reduced emission of pollutants. PEFCs are already commercialized for residential cogeneration systems and transportation applications in Japan [1]. For example, Enefarm Systems, which is the home cogeneration system of 1 kW polymer electrolyte fuel cell systems, was commercialised in 2009. An accumulated amount of Enefarm systems reached 250,000 at July in 2018 in Japan. In addition, the fuel cell vehicle named MIRAI with 100 kW PEFC stack manufactured by TOYOTA motor corporation was also commercialized at the end of 2014 in Japan. However, its cost is still high (Approximately 7 million yen), thus hindering their widespread commercialization. One of the reasons of its high cost is the use of platinum as electrocatalysts (Typical Pt/C state-of-the-art cathode loading is several ten grams), especially on the cathode side. Because an oxygen reduction reaction (ORR) at the cathode has a large overpotential, a relatively large amount of platinum is loaded to promote the ORR. Therefore, to successfully commercialize PEFCs, low-cost non-platinum cathode catalysts must be developed.

Many researchers have investigated iron- and/or cobalt-complex–based catalysts such as Fe–N–C, that feature high ORR activities comparable to that of platinum-based catalysts [2]. Despite significant enhancements of the ORR activity of iron-based non-platinum catalysts, issues regarding their long-term durability remain unsolved. We have focused on group 4 and 5 metal oxide-based compounds because of their high stability even in acidic media. Recently, we successfully synthesized oxide-based nanoparticles using oxy-metal

phthalocyanines (MeOPc; Me = Ta, Zr, and Ti) as starting material and multi-walled carbon nanotubes (MWCNTs) as the support and electro-conductive material [3-5]. We revealed that phthalocyanine-derived deposited carbon played a role in creating the ORR-active oxygen vacancy sites near the oxide surface and in promoting ORR by providing local nanoscale electrical conduction paths on the relatively insulating oxide surfaces [6]. However, carbon materials are easily oxidized at high potentials with a consequent decrease of the ORR activity due to degradation of the electron supply paths [7]. Thus, carbon-free electrocatalysts are required in order to achieve high durability of the oxide-based cathodes. The carbon-free electrocatalysts must consist of two kinds of oxides, i.e., oxides having active sites for the ORR and electro-conductive oxides. In order to obtain sufficient ORR activity of carbon-free oxides, it is necessary to separately optimize the conditions for the formation of oxides with active sites and the formation of electro-conductive oxides. We already prepared two model catalysts to reveal the factors that affected the ORR activity of niobium-doped titanium oxides. One is a thin film composed of titanium-niobium oxides on a glassy carbon rod as a substrate [8], and another consists of nano-sized Nb_2O_5-doped TiO_2 particles supported on the MWCNTs [9]. We successfully found that the heat-treatment under a reductive atmosphere was useful to produce the localized electron energy levels and the crystalline distortion of the anatase phase might be essential to show the ORR activity. However, in both cases we used carbon materials such as glassy carbon and MWCNTs to have sufficient electrical conductivity. The carbon materials were heat-treated simultaneously with the oxides to generate the ORR activity. Thus, the effect of the existence of carbon materials

during the heat-treatment on the emergence of the ORR activity could not be completely excluded. We need to evaluate the ORR activity of the oxides themselves.

Because the oxides with the ORR activity were almost insulators, we firstly needed to develop the evaluation method of the ORR activity in the oxides. We attempted to use a mixture of the oxides with carbon black powder as an electro-conductive additive to evaluate the electrochemical behavior of the oxides. Although the carbon black powder was used, the oxides were heat-treated without carbon materials and carbon black only formed electron conduction paths near the surface of the oxides.

In this study, we firstly developed the evaluation method of the electrochemical behavior of the oxides by the addition of carbon black as an electro-conductive material. Using the developed method, we focused on the effect of niobium addition into titanium oxides on the formation of active sites using a high concentration sol-gel method. The correlation between an amount of added niobium and the ORR activity, the physico-chemical properties in the absence of a carbon support are discussed.

2. Experimental

The high concentration sol-gel method [10,11] was used for the preparation of the precursor. A volume of 30 cm^3 of titanium(IV) tetraisopropoxide ($C_{12}H_{28}O_4Ti$, 99.99%, Aldrich) and 0, 2.8, 6.3, and 10.8 cm^3 of niobium(V) ethoxide ($C_{10}H_{25}NbO_5$, 99.95%, Aldrich) were dissolved in 200 cm^3 of 2-methoxyethanol with Ti:Nb atomic ratios of 10:0, 9:1, 8:2, and 7:3, respectively. Thus, we prepared samples with Nb mole percentages of 0, 10, 20, and 30 mol%, respectively. The mixed solutions were maintained at -50 °C, and

mixtures of 2-methoxyethanol and pure water with equivalent volumes of 29, 32, 36, and 41 cm^3 were added to the mixed solutions dropwise, respectively. The amount of added water was enough to precipitate as oxides. The temperature of the solution was raised to 80 °C and maintained for 3 weeks as an aging treatment, resulting in the formation of nano-sized complex oxides. The precipitates were mixed with 2-methoxyethanol to obtain a dispersion of nano-sized titanium-niobium oxide.

The dispersion was dried on a Teflon tray heated at 160 °C to obtain niobium-added titanium oxide powders. To remove organic species and carbon residue, the powder was heat-treated at 380 °C for 3 h in air as a pre-heat-treatment step. Subsequently, samples of niobium-added titanium oxide powders were heat-treated at 700 °C in Ar containing 4% H_2 for 10 min to prepare the catalysts. Figure 1 shows the schematic drawing of the synthetic procedure. These catalysts were denoted 0mol%Nb-TiO_2, 10mol%Nb-TiO_2, 20mol%Nb-TiO_2, and 30mol%Nb-TiO_2, respectively.

The Brunauer–Emmett–Teller (BET) specific surface area of the synthesized catalysts was determined by nitrogen adsorption (BELSORP-mini, Microtrac BEL). The microstructure of the catalysts was analyzed by transmission electron microscopy (TEM, JEOL LEM-2100F), and selected-area electron diffraction (SAED). The crystalline structures, and chemical states of the synthesized catalysts were investigated by X-ray diffraction (XRD; Rigaku Ultima IV, X-ray source: Cu-Kα) and X-ray photoelectron spectroscopy (XPS; PHI Quantum-2000, X-ray source: monochromated Al-Kα radiation). The peak of the C–C bond attributed to free carbon at 284.6 eV in the C 1s spectrum was used to compensate for surface charging.

The apparent electrical conductivity of the catalyst powders was measured under an ambient air atmosphere using the two probes method. The catalyst powders were placed into a cylinder with a radius of 5.0 mm, and aluminum foil electrodes were placed at the top and bottom of the column of the catalyst powder. The electrical resistance was measured under an applied pressure (60 MPa) with a DC resistivity analyzer (Resistance Meter, RM3545, HIOKI).

We used a stationary electrode system to evaluate the ORR current in a kinetically controlled region, i.e. a high potential region, instead of a rotating ring-disk electrode [12]. We already confirmed that the ORR currents observed in the high potential region using a stationary electrode system and a rotating ring-disk electrode are the same.

A certain weight of Ketjenblack EC300J (KB) from ca. 0.18 to 0.5 mg was mixed with catalyst powder of 3 mg to examine the effect of the KB-to-oxide ratio on the electrochemical behavior of oxides. Then, the mixed powder was dispersed into a 1:1 (mass ratio) solution of 1-propanol and distilled water (0.15 cm^3) with 0.5-wt%Nafion® solution (0.005 cm^3) to prepare a catalyst ink. The catalyst ink was repeatedly dropped on a polished glassy carbon rod (GC; φ = 5.2 mm, TOKAI CARBON CO., LTD.) and dried at 60 °C until the powder was supported, at a loading of ~0.1 mg cm^{-2}, on top of the GC to prepare the working electrode. In addition, the working electrode, loaded with pure KB at a certain weight, was also prepared to evaluate the electrical double layer capacitance of the oxides.

Stationary electrode measurements were performed with a 3-electrode cell in 0.1 M H_2SO_4 (for Volumetric Analysis, Factor = 1.000, FUJIFILM Wako Pure Chemical, Ltd.) at 30 °C. An RHE and a glassy carbon plate were used as the reference and counter electrodes,

respectively. A potentiostat (PS08, TOHO Technical Research) was used. Cyclic voltammetry was performed with different potential scan rate to evaluate the influence of the scan rate on the shape and magnitude of cyclic voltammograms (CVs). To evaluate the electrical double layer capacitance of the oxides, we obtained the CVs of the KB-oxide mixture and pure KB. The double layer capacitance was evaluated in the potential range from 0.8 to 1.0 V vs. RHE because no Faradaic peaks were observed in the potential range. The double layer capacitance of the oxide was obtained by subtracting the capacitance of the pure KB from the mixture of the oxide and KB.

Slow scan cyclic voltammetry was performed at a scan rate of 5 mV s^{-1} from 0.2 to 1.2 V under O_2 and N_2 atmospheres to obtain the ORR current density. The purity of N_2 and O_2 gases was higher than 99.99995% and 99.5%, respectively. The ORR current density, j_{ORR}, based on the oxide mass (mass activity), was determined by calculating the difference between the current density under an O_2 and an N_2 atmosphere.

3. Results and Discussion

3.1. Conductivity, specific surface area and crystalline structure of Nb-TiO_2 catalysts

Fig.2 shows the dependence of (a) the conductivity after heat-treatment at 700 °C for 10 min under 4%H_2/Ar and (b) the specific surface area before and after the heat-treatment at 700 °C for 10 min under 4%H_2/Ar of the niobium-added titanium oxides on the Nb mole percentage. The specific surface areas of the niobium-added titanium oxides, i.e., precursors, before the heat-treatment at 700 °C for 10 min were almost the same and quite high, namely 111, 110, 107, and 106 m^2 g^{-1}, respectively. The specific surface area after the heat-treatment

at 700 °C for 10 min drastically decreased in all samples. In particular, the specific surface area of 0mol%Nb-TiO_2 was extremely low and the decrease of the specific surface area of Nb-added TiO_2 due to the heat-treatment was restrained. This resulted in the increase of the specific surface area after the heat-treatment at 700 °C for 10 min, with the increasing in the Nb mole percentage up to 20 and almost remaining constant.

On the other hand, the conductivities of the oxides before the heat-treatment at 700 °C for 10 min as low as an insulator; thus, we were unable to evaluate these conductivities. The 0mol%Nb-TiO_2 catalyst showed very low conductivity. The conductivity increased one order of magnitude when increasing the Nb mole percentage up to 10, and remained almost constant above 10mol%.

It is well known that the doping of Nb ions into the titanium oxide structure leads to the restraint of phase transformation from anatase to rutile [13,14] and the increase in the conductivity by the creation of local electron energy levels among the band bap [15-17]. Fig. 3 shows the XRD patterns of the catalysts with (a) a scan range of 20 – 90° and (b) a narrow range of 24 – 28°. All precursors before the heat-treatment at 700 °C for 10 min showed anatase structure. However, as shown in Fig.3 (a), the 0mol%Nb-TiO_2 had both anatase and rutile phases, indicating that the phase transformation from anatase to rutile proceeded during the reductive heat-treatment at 700 °C for 10 min. On the other hand, the other catalysts show peaks identified as the anatase phase. The Nb addition clearly demonstrated the restraint of phase transformation from anatase to rutile. As shown in Fig.3 (b), the main peak of the anatase phase due to (1 0 1) at 25.280° (JCPDS no. 00-021-1272) shifted to lower angles as the Nb mole percentage increased. This peak shift for lower angles was responsible for a

lattice expansion of anatase phase. Because the Shannon ionic radii of Nb^{5+} (64 pm) is slightly larger than that of Ti^{4+} (60.5 pm) for a coordination number of six [18], it is reasonable that substitution with Nb causes the peak to shift to lower angles. Thus, the peak shift to lower angles suggests that the amount of doped Nb into the anatase phase increased as the amount of Nb addition increased. The phase transformation to rutile phase caused the decrease in the specific surface area. This is the reason why the specific surface area of the 0mol%Nb-TiO_2 is so small. Up to the Nb mole percentage of 20, the decrease in the specific surface area was restrained by the substitution of Nb ions into the anatase phase.

Regarding the conductivity, it is also well known that Nb doping enhances the conductivity of the anatase phase [19,20]. Thus, the drastic increase in the conductivity from 0 to 10 mol% was responsible for the Nb doping into the anatase structure. Although the Nb doping increased with the increase in the Nb mole percentage, the conductivity remained constant above Nb mole percentage of 10. Thus, the other phenomena such as the formation of titanium-niobium complex oxides and/or amorphous niobium oxides might occurred simultaneously with the substitution of Nb ions to Ti ions. This behavior will be discussed in next section using TEM images and SAED.

3.2. Electronic and surface state of the Nb-TiO_2 catalysts

Fig. 4 shows the (a) Ti 2p and (b) Nb 3d XPS spectra of the Nb-TiO_2 catalysts. The Ti 2p XPS spectra revealed that Ti adopted the tetravalent state for the 0mol%Nb-TiO_2 based on the $2p_{3/2}$ peak (TiO_2; 458.8 eV [21]). On the other hand, a low valence state, i.e., Ti^{3+} (Ti_2O_3; 456.8 eV [22]), was clearly observed for the 10, 20, and 30mol%Nb-TiO_2. Fig. 4 (c)

shows the dependence of the ratios of $Ti^{3+}/(Ti^{4+}+Ti^{3+})$, i.e., $S_{Ti(III)}/(S_{Ti(IV)}+S_{Ti(III)})$ calculated from areas of the Ti 2p spectra of the Nb-TiO_2 catalysts on the mole percentage of Nb. Even in the 0mol%Nb-TiO_2, ca. 5 mol% Ti^{3+} were produced because of the reductive heat-treatment. The ratio of $Ti^{3+}/(Ti^{4+}+Ti^{3+})$ increased when increasing the Nb mole percentage, especially drastically increased from 20 to 30. Because Ti^{3+} ions are produced by the substitution of the Nb^{5+} ions with Ti^{4+} ions of the TiO_2 lattice, the increase in the Nb mole percentage of Nb led to the increase in the ratio of $Ti^{3+}/(Ti^{4+}+Ti^{3+})$.

On the other hand, as shown in Fig. 4 (b), the peaks in the Nb 3d spectra of the 10 and 20mol%Nb-TiO_2 corresponded to Nb_2O_5, whereas the 3d peak of the 30mol%-TiO_2 shifted to lower binding energy (NbO_2; 205.1 eV [23], Nb_2O_5; 206.8 eV [23]). These results suggest that a low valence state, i.e., Nb^{4+}, was produced in the 30mol%Nb-TiO_2.

Table 1 summarizes the Ti-element mole ratio to Ti and content with a unit of mol% of each sample. The ratios of Nb to (Ti + Nb) near the surface were also included. The atomic ratios of Nb/(Ti+Nb) calculated from areas of the XPS spectra of the 10, 20, and 30mol%Nb-TiO_2 were 0.15, 0.28, and 0.43, respectively. These ratios are larger than the total atomic ratio, in particular, 30mol%Nb-TiO_2, suggesting that the niobium ions accumulated in the surface of the oxide particles. To investigate the surface of the oxide particles, TEM observation and SAED were performed in each catalyst.

Fig. 5 shows the TEM images of (a) 0mol%Nb-TiO_2, (b) 10mol%Nb-TiO_2, (c) 20mol%Nb-TiO_2, and (d) 30mol%Nb-TiO_2, respectively. As shown in Fig. 5 (a), some large particles with a diameter of several hundred nanometers and no amorphous layer on the surface of the small particles were observed in the case of the 0mol%Nb-TiO_2. This particle

growth corresponded to the drastic decrease in the specific surface area of the 0mol%Nb-TiO_2. In case of the 10 mol%Nb-TiO_2, as shown in Fig. 5 (b), most of the particles had a diameter of tens of nanometers. The surface of the particles had fine irregularity and no amorphous layer was observed on the surface. It was confirmed that the Nb doping restrained the particle growth by the restraint of the phase transformation. The specific feature of the 10 mol%Nb-TiO_2 was the observation of fine particles with a diameter of ca. 1 nm, as shown with an arrow in the images. In the case of the 20 mol%Nb-TiO_2, as shown in Fig. 5 (c), the particle size was approximately tens of nanometers. However, the surface of the particles was relatively smooth and an amorphous phase was observed on the surface. In addition, no fine particles with a diameter of ca. 1 nm were observed. In case of the 30 mol%Nb-TiO_2, as shown in Fig. 5 (d), the surface of the oxides was also smooth and an amorphous phase was also observed.

SAED was performed to reveal the materials and local crystalline structure of each catalyst. Fig. 6 shows the TEM images and corresponding SAED of (a1) and (a2) 0mol%Nb-TiO_2, (b) 10mol%Nb-TiO_2, (c) 20mol%Nb-TiO_2, and (d) 30mol%Nb-TiO_2. Although only anatase and rutile phases were observed in the XRD patterns, many kinds of oxides were detected by the SAED. Fig. 6 (a2) shows the large particle of the 0mol%Nb-TiO_2 and its SAED, indicating that the large particle was composed of rutile. The transformation from anatase to rutile promoted the particle growth, thus decreasing the specific surface area. The SAED of the 0mol%Nb-TiO_2 revealed that brookite and Ti_4O_7 phases also existed together with anatase and rutile, as shown in Fig. 6 (a1). Because the heat-treatment was performed

under a reductive atmosphere, i.e., 4%H_2/Ar, TiO_2 was reduced to low valence titanium oxides such as Ti_4O_7.

Fig. 6 (b) and (c) suggest that the 10mol%Nb- and 20mol%Nb-TiO_2 were mainly composed of anatase, Ti_4O_7, and $TiNb_2O_7$. Because the Nb mole percentage increased, the niobium-titanium complex oxide $TiNb_2O_7$, was produced during the heat-treatment. In case of the 30mol%Nb-TiO_2, as shown in Fig. 6 (d), Nb ions were unable to substitute the anatase phase and produce $TiNb_2O_7$ to form the Nb_2O_5 phase, because of the excess amount of Nb. It was considered that the amorphous layer on the surface was amorphous-like Nb_2O_5 phase. This result was supported by the large atomic ratios of Nb/(Ti+Nb) near the surface as shown in Table 1.

3.3. Evaluation of electrochemical behavior of Nb-TiO_2 catalysts

Fig. 7 (a) shows the cyclic voltammogram (CV) of the mixture of 10mol%Nb-TiO_2 and KB with a weight ratio of 10:1 (red line), the CV of the pure KB with equivalent weight in the mixture (pink line), and the CV of the pure 10mol%Nb-TiO_2 with equivalent weight in the mixture (blue line) in 0.1 M H_2SO_4 at 30 °C under inert atmosphere. The CV of the pure 10mol%Nb-TiO_2 was very small because the conductivity of the 10mol%Nb-TiO_2 was low, ca. 2×10^{-6} S cm^{-1}. On the other hand, the CV of the mixture of 10mol%Nb-TiO_2 and KB was apparently larger than those of pure KB or pure 10mol%Nb-TiO_2. Because the weight of KB in the loading on the GC rod was the same, the difference of the CVs between mixture and pure KB was attributed to the 10mol%Nb-TiO_2. The increase in the CV suggests that the surface of the 10mol%Nb-TiO_2 could be electrochemically activated by the

formation of an electron conduction network based on the mixed KB. Thus, even if the oxide catalysts are almost insulators, that is, the CVs of the pure oxide catalysts are very small, the mixture of KB with the oxide catalysts can activate the oxide surface by the formation of the electron conduction network from outside of the oxides. Therefore, we were able to evaluate the double layer capacitance relative to the oxides by the current in the potential range from 0.8 to 1.0 V. As shown in Fig. 7 (a), the area of the difference between the red and blue lines (green area) is responsible for the specific surface area of the 10mol%Nb-TiO_2. We can thus evaluate the double layer capacitance relative to the oxides by the addition of KB as electro-conductive materials. We examined the effect of the KB ratio in the mixture on the capacitance.

Fig. 7 (b) shows the dependence of the capacitance based on the oxide mass on the weight of the mixed KB when the weight of the 10mol%Nb-TiO_2 was fixed at 3.0 mg. As shown in Fig. 7 (b), the capacitance based on the oxide mass was independent of the weight of the mixed KB, suggesting that the electron conduction network composed of KB on the oxide surface was already formed by a small amount of additional KB. Therefore, we chose the oxide-to-KB mixing ratio as 10:1, i.e., oxide powder; 3.0 mg + KB; 0.3 mg. Next, to accurately evaluate the capacitance of the oxides from the CVs, we investigated the effect of the potential scan rate on the capacitance of the oxides.

Fig. 8 (a) shows the effect of a potential scan rate on the CVs of the mixture of 10mol%Nb-TiO_2 and KB with a weight ratio of 10:1. As shown in Fig. 8 (a), the CVs showed similar shape. Fig. 8 (b) showed the dependence of the potential scan rate on the capacitance calculated from the CVs in the potential range from 0.8 to 1.0 V. When the scan rate was low,

some Faradaic currents might be included to slightly increase the capacitance. On the other hand, the capacitance of the oxides almost remained constant in a scan rate from 50 to 150 mV s^{-1}. Therefore, we chosen 150 mV s^{-1} as the scan rate to obtain the capacitance of the oxides.

Fig. 9 (a) showed the dependence of the capacitance of the oxide catalysts based on oxide mass on the Nb mole percentage. The dependence was similar to that of the specific surface area of the oxides, as shown in Fig. 2 (b). We plotted the capacitance and the specific surface area of the oxides, as shown in Fig. 9 (b). A linear relation was obtained, suggesting that the capacitance was governed by the specific surface area of the oxides. Fig. 9 (c) shows the dependence of the capacitance based on the specific surface area on the Nb mole percentage. The capacitance based on the specific surface area was independent of the Nb mole percentage. Thus, there was no influence of the amount of added Nb on the capacitance of the oxides.

We evaluated the ORR activity of the oxide catalysts using the KB-oxide mixture. First, we confirmed the effect of the weight of the mixed KB on the ORR current based on the oxide mass. Fig. 10 (a) shows the dependence of the ORR current density based on the mass of the 10mol%Nb-TiO_2 on the weight of mixed KB when the weight of the 10mol%Nb-TiO_2 was fixed at 3.0 mg. Similar to Fig. 9 (c), the ORR current density based on the mass of the 10mol%Nb-TiO_2 was independent of the weight of the mixed KB, suggesting that the ORR activity of the 10mol%Nb-TiO_2 could be evaluated by the KB mixture as well as by the capacitance. We evaluated the ORR activities of the oxides by the mixture of KB with the ratio of the 10mol%Nb-TiO_2 and the KB with a weight ratio of 10:1.

Fig. 10 (b) shows the potential-ORR current curves for the ORR of the mixture of KB and catalysts in 0.1 M H_2SO_4 at 30 °C. The ORR current of the pure KB started to flow below ca. 0.6 V, indicating that the observed ORR activity was responsible for the oxide catalysts. The specific surface area, i.e., the double layer capacitance of the oxides, affected the ORR current. Thus, to exclude the effect of the specific surface area, the ORR current densities were based on the double layer capacitance of the oxides.

Fig. 10 (c) shows the dependence of the ORR current density at 0.7 V based on the capacitance of the Nb-TiO_2, $|j_{ORR}@0.7V|$, on the Nb mole percentage in 0.1 M H_2SO_4 at 30 °C. The $|j_{ORR}@0.7V|$ of the 0mol%Nb-TiO_2 was almost zero, indicating that the onset potential for the ORR of this oxide was lower than 0.7 V, that is, the 0mol%Nb-TiO_2 had lower ORR activity. The $|j_{ORR}@0.7V|$ drastically increased with the increasing Nb mole percentage up to 10 and remained constant above 20mol%. This result demonstrates that the Nb doping is effective to enhance the ORR activity of titanium oxide-based cathodes. However, the Nb doping excess 10mol% hardly enhanced the ORR activity. We already performed XPS, TEM and SAED to elucidate the reason of this behavior.

The relationship between the $|j_{ORR}@0.7V|$ and the ratio of $Ti^{3+}/(Ti^{4+}+Ti^{3+})$ obtained by Ti 2p XPS spectra (Fig. 4) was plotted as shown in Fig. 11. The linear relation was observed below the 20mol%Nb-TiO_2, i.e., the ratio of $Ti^{3+}/(Ti^{4+}+Ti^{3+})$ of ca. 12%. We found that the Ti^{3+} and/or oxygen vacancies might affect the ORR activity [9]. Thus, the increase in the ORR activity below the 20mol%Nb-TiO_2 was responsible for the increase in the Ti^{3+} and/or oxygen vacancies. In the case of the 30mol%Nb-TiO_2, although the ratio of $Ti^{3+}/(Ti^{4+}+Ti^{3+})$ reached 28%, the ORR activity still remained. As discussed in the previous section, in case

of the 30mol%Nb-TiO_2, Nb ions were unable to substitute the anatase phase and produce $TiNb_2O_7$ to form the amorphous-like Nb_2O_5 layer, because of the excess amount of Nb. We think that the amorphous-like Nb_2O_5 layer had low ORR activity. Thus, the ORR activity of the 30mol%Nb-TiO_2 was almost the same as that of the 20mol%Nb-TiO_2, although the ratio of the $Ti^{3+}/(Ti^{4+}+Ti^{3+})$ of the 30mol%Nb-TiO_2 was larger than that of the 20mol%Nb-TiO_2.

According to the results, we can understand this behavior, as shown in Fig. 10 (c) as follows: the increase in the ORR activity in the Nb mole percentage from 0 to 20 was attributed to the increase in the ratio of the $Ti^{3+}/(Ti^{4+}+Ti^{3+})$. Although the ratio of the $Ti^{3+}/(Ti^{4+}+Ti^{3+})$ of the 30mol%Nb-TiO_2 was much larger than that of the 20mol%Nb-TiO_2, the amorphous phase composed of Nb_2O_5 deposited as a thin layer on the surface of the particles, which had low ORR activity to hinder the emergence of the ORR activity.

Tafel plots of the Pt/C, $TiC_xN_yO_z$/MWCNT [5], and 20mol%Nb-TiO_2 were compared in Fig. S1. Because of the low electrical conductivities of the Nb-doped TiO_2 powders, it is difficult to obtain the large ORR current. While, when carbon such as multi-walled carbon nanotube is used for electro-conductive support, the relatively large ORR current is obtained as shown in Fig.S1 for the $TiC_xN_yO_z$/MWCNT even the $TiC_xN_yO_z$/MWCNT doesn't contain Nb. Thus, we're going to enhance the ORR activity of the $TiC_xN_yO_z$/MWCNT using Nb doping to approach the Pt/C.

4. Conclusions

In order to evaluate the electrochemical behavior such as the double layer capacitance and the ORR activity of oxide catalysts that had low electrical conductivity, we attempted to

mix the Ketjenblack as electro-conductive material with oxide catalysts. The appropriate mixture of the KB with the oxide catalysts led to the electrochemical activation of the oxide surface by the formation of electron conduction networks. Using the KB mixture, we focused on the niobium added titanium oxides heat-treated at 700 °C for 10 min under 4%H_2/Ar without carbon materials to reveal the dependence of the ORR activity on the Nb mole percentage. The ORR activity of the Nb-TiO_2 increased in the Nb mole percentage from 0 to 20. This increase was due to the increase in the ratio of the $Ti^{3+}/(Ti^{4+}+Ti^{3+})$, suggesting that the active sites were Ti^{3+} and/or oxygen vacancies in the anatase phase. On the other hand, although the ratio of the $Ti^{3+}/(Ti^{4+}+Ti^{3+})$ of the 30mol%Nb-TiO_2, 28%, was much larger than that of the 20mol%Nb-TiO_2, 12%, the ORR activities were almost the same. This might be responsible for the deposition of the amorphous phase composed of Nb_2O_5, which, as a thin layer on the surface of the particles, had low ORR activity.

Acknowledgments

The authors acknowledge financial support from the New Energy and Industrial Technology Development Organization (NEDO). This work was conducted under the auspices of the Ministry of Education, Culture, Sports, Science and Technology (MEXT) Program for Promoting the Reform of National Universities. The project was also funded by JSPS Research Fund JP18K05291, the Suzuki Foundation, and the Tonen General Petroleum Research Encouragement and Scholarship Foundation.

References

[1] Sasaki K. Part I General Introduction. In: Sasaki K, Li H.-W., Hayashi A, Yamabe J, Ogura T, M. Lyth S, editors. Hydrogen Energy Engineering A Japanese Perspective, Springer Japan; 2016, p.15-35. DOI 10.1007/978-4-431-56042-5

[2] Martinez U, Babu S, K, Holby, E. F, Chung H. T, Yin Xi, Zelenay P. Progress in the Development of Fe-Based PGM-Free Electrocatalysts for the Oxygen Reduction Reaction. Adv. Mater. 2019;1806545. https://doi.org/10.1002/adma.201806545

[3] Ishihara A, Chisaka M, Ohgi Y, Matsuzawa K, Mitsushima S, Ota K. Synthesis of nano-TaO_x oxygen reduction reaction catalysts on multi-walled carbon nanotubes connected via a decomposition of oxy-tantalum phthalocyanine. Phys. Chem. Chem. Phys. 2015;17; 7643-7647. DOI: 10.1039/C5CP00317B

[4] Chisaka M, Ishihara A, Morioka H, Nagai T, Yin S, Ohgi Y, Matsuzawa K, Mitsushima S, Ota K. Zirconium Oxynitride-Catalyzed Oxygen Reduction Reaction at Polymer Electrolyte Fuel Cell Cathodes. ACS Omega 2017;2;678-684. DOI: 10.1021/acsomega.6b00555

[5] Tominaka S, Ishihara A, Nagai T, Ota K. Non-crystalline Titanium Oxide Catalysts for Electrochemical Oxygen Reduction Reactions. ACS Omega 2017;2;5209−5214. DOI: 10.1021/acsomega.7b00811

[6] Ishihara A. Nagai T. Ukita K. Arao M. Matsumoto M. Yu L. Nakamura T. Sekizawa O. Takagi Y. Matsuzawa K. Napporn W. T. Mitsushima S. Uruga T. Yokoyama T. Iwasawa Y. Imai H. Ota K. J. Phys. Chem. C, in press,
https://pubs.acs.org/doi/10.1021/acs.jpcc.9b02393

[7] Okada Y. Ishihara A. Matsumoto M. Imai H. Kohno Y. Matsuzawa K. Mitsushima S. Ota K. Effect of Reheating Treatment on Oxygen-Reduction Activity and Stability of Zirconium Oxide-Based Electrocatalysts Prepared from Oxy-Zirconium Phthalocyanine for Polymer Electrolyte Fuel Cells. J. Electrochem. Soc. 2015;162;F959-F964. doi: 10.1149/2.0201509jes

[8] Ishihara A. Tamura Y. Kohno Y. Matsuzawa K. Mitsushima S. Ota K. Titanium-niobium oxides as non-precious metal cathodes for polymer electrolyte fuel cells. Catalysts 2015;5(3);1289-1303. https://doi.org/10.3390/catal5031289

[9] Ishihara A. Wu C. Nagai T. Ohara K. Nakada K. Matsuzawa K. Napporn W. T. Arao M. Kuroda Y. Tominaka S. Mitsushima S. Imai H. Ota K. Factors affecting oxygen reduction activity of Nb_2O_5-doped TiO_2 using carbon nanotubes as support in acidic solution. Electrochim. Acta 2018;283;1779-1788. https://doi.org/10.1016/j.electacta.2018.07.082

[10] Matsuda H. Mizushima T. Kuwabara M. Low-Temperature Synthesis and Electrical Properties of Semiconducting $BaTiO_3$ Ceramics by the Sol-Gel Method with High Concentration Alkoxide Solutions. J. Ceram. Soc. Jpn. 1999;107;290-292. https://doi.org/10.2109/jcersj.107.290

[11] Matsuda H. Kobayashi N. Kobayashi T. Miyazawa K. Kuwabara M. Room-temperature synthesis of crystalline barium titanate thin films by high-concentration sol-gel method. J. Non-cryst. Solids 2000;271;162-166. https://doi.org/10.1016/S0022-3093(00)00101-0

[12] Ohgi Y. Ishihara A. Matsuzawa K. Mitsushima S. Matsumoto M. Imai H. Ota K. Oxygen reduction reaction on tantalum oxide-based catalysts prepared from TaC and TaN. Electrochim. Acta 2012;68;192-197. https://doi.org/10.1016/j.electacta.2012.02.059

[13] Arbiol J. Cerdà J. Dezanneau G. Cirera A. Peiró F. Cornet A. Morante J. R. Effects of Nb doping on the TiO_2 anatase-to-rutile phase transition. J. Appl. Phys. 2002;92;853-861. https://doi.org/10.1063/1.1487915

[14] Guidi V. Carotta M. C. Ferroni M. Martinelli G. Effect of Dopants on Grain Coalescence and Oxygen Mobility in Nanostructured Titania Anatase and Rutile. J. Phys. Chem. B 2003;107;120–124. DOI: 10.1021/jp013572u

[15] Dy E. Hui R. Zhang J. Liu Z.-S. Shi Z. Electronic Conductivity and Stability of Doped Titania ($Ti_{1-X}M_XO_2$, M=Nb, Ru, and Ta)—A Density Functional Theory-Based Comparison. J. Phys. Chem. C 2010;11413162–13167. DOI: 10.1021/jp100826g

[16] Morris D. Dou Y. Rebane J. Mitchell C. E. J. Egdell R. G. Law D. S. L. Vittadini A. Casarin M. Photoemission and STM study of the electronic structure of Nb-doped TiO_2. Phys. Rev. B 2000;61;13445. https://doi.org/10.1103

[17] Song K. Han X. Shao G. Electronic properties of rutile TiO_2 doped with 4d transition metals: First-principles study. J. Alloys Compd. 2013;551;118-124. https://doi.org/10.1016/j.jallcom.2012.09.077

[18] Shannon R.D. Revised effective ionic radii and systematic studies of inter-atomie distances in halides and chaleogenides. Acta Crystallogr. 1976;A32;751. https://doi.org/10.1107/S0567739476001551

[19] Furubayashi Y. Yamada N. Hirose Y. Yamamoto Y. Otani M. Hitosugi T. Shimada T. Hasegawa T. Transport properties of d-electron-based transparent conducting oxide: Anatase $Ti_{1-x}Nb_xO_2$. J. Appl. Phys. 2007;101;093705. https://doi.org/10.1063/1.2721748

[20] Furubayashi Y. Hitosugi T. Yamamoto Y. Inaba K. Kinoda G. Hirose Y. Shimada T. Hasegawa T. A transparent metal: Nb-doped anatase TiO_2. Appl. Phys. Lett. 2005;86;252101. https://doi.org/10.1063/1.1949728

[21] Haukka S. Lakomaa E.-L. Jylha O. Vilhunen J. Hornytzkyj S. Dispersion and Distribution of Titanium Species Bound to Silica from $TiCl_4$. Langmuir 1993;9;3497-3506. https://pubs.acs.org/doi/pdf/10.1021/la00036a026

[22] González-Elipe A.R. Munuera G. Espinos J.P. Sanz J.M. Compositional changes induced by 3.5 keV Ar^+ ion bombardment in Ni-Ti oxide systems: A comparative study. Surf. Sci. 1989;220;368-380. https://doi.org/10.1016/0039-6028(89)90239-2

[23] Khoviv D. A. Zaytsev S. V. Ievlev V.M. Thin Solid Films 2012;520;4797-4799. https://doi.org/10.1016/j.tsf.2011.10.130

Figure captions

Fig.1 Schematic drawing of the synthetic procedure.

Fig. 2 Dependence of (a) the conductivity after heat-treatment at 700 °C for 10 min under 4%H_2/Ar and (b) the specific surface area before and after heat-treatment at 700 °C for 10 min under 4%H_2/Ar of the titanium-niobium oxides on the Nb mole percentage.

Fig. 3 XRD patterns of the catalysts with (a) a scan range of 20 – 90° and (b) a narrow range of 24 – 28°.

Fig. 4 (a) Ti 2p and (b) Nb 3d XPS spectra of the Nb-TiO_2 catalysts. (c) Dependence of the ratios of $Ti^{3+}/(Ti^{4+}+Ti^{3+})$, $S_{Ti(III)}/(S_{Ti(IV)}+S_{Ti(III)})$ calculated from areas of the Ti 2p spectra of the Nb-TiO_2 catalysts on the mole percentage of Nb.

Fig. 5 TEM images of (a) 0mol%Nb-TiO_2, (b) 10mol%Nb-TiO_2, (c) 20mol%Nb-TiO_2, and (d) 30mol%Nb-TiO_2.

Fig. 6 TEM images and corresponding SAED of (a1) and (a2) 0mol%Nb-TiO_2, (b) 10mol%Nb-TiO_2, (c) 20mol%Nb-TiO_2, and (d) 30mol%Nb-TiO_2.

Fig. 7 (a) Cyclic voltammogram (CV) of the mixture of 10mol%Nb-TiO_2 and KB with a weight ratio of 10:1 (red line) and CV of the pure KB with equivalent weight in the mixture (pink line) and CV of the pure 10mol%Nb-TiO_2 with equivalent weight in the mixture (blue line) in 0.1 M H_2SO_4 at 30 °C under inert atmosphere. (b) Dependence of the capacitance based on the oxide mass on the weight of mixed KB when the weight of the 10mol%Nb-TiO_2 was fixed at 3.0 mg.

Fig. 8 (a) Effect of a potential scan rate on the CVs of the mixture of 10mol%Nb-TiO_2 and KB with a weight ratio of 10:1. (b) Dependence of the potential scan rate on the capacitance calculated from the CVs in the potential range from 0.8 to 1.0 V.

Fig. 9 (a) Dependence of the capacitance of the oxide catalysts on the Nb mole percentage, (b) Relationship between double layer capacitance based on mass of oxides and specific surface area, (c) Dependence of the capacitance based on specific surface area on the Nb mole percentage.

Fig. 10(a) Dependence of the ORR current density based on the mass of the 10mol%Nb-TiO_2 on the weight of mixed KB when the weight of the 10mol%Nb-TiO_2 was fixed at 3.0 mg, (b) Potential-ORR current curves for the ORR of the mixture of KB and catalysts, and (c) Dependence of the ORR current density at 0.7 V based on the capacitance of the Nb-TiO_2, $|j_{ORR}@0.7V|$, on the Nb mole percentage in 0.1 M H_2SO_4 at 30 °C.

Fig. 11 Relationship between the $|j_{ORR}@0.7V|$ and the ratio of $Ti^{3+}/(Ti^{4+}+Ti^{3+})$.

Table 1 Ti-element mole ratio of element to Ti, the content with a unit of mol%, and the atomic ratios of Nb/(Ti+Nb) near the surface of each sample.

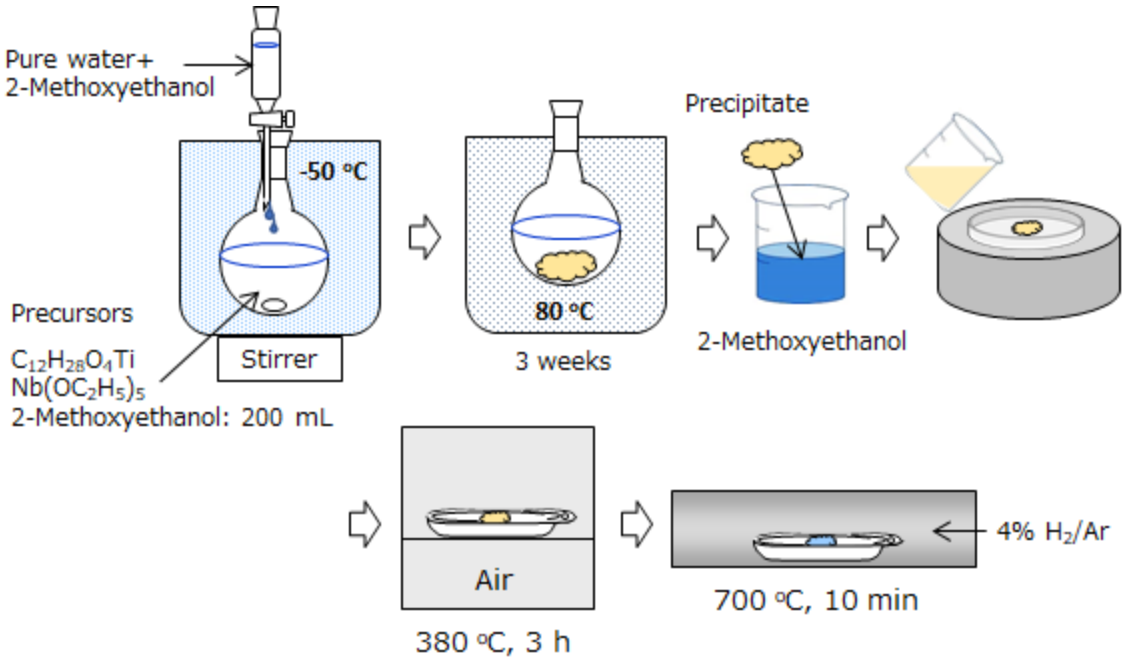

Fig.1 Schematic drawing of the synthetic procedure.

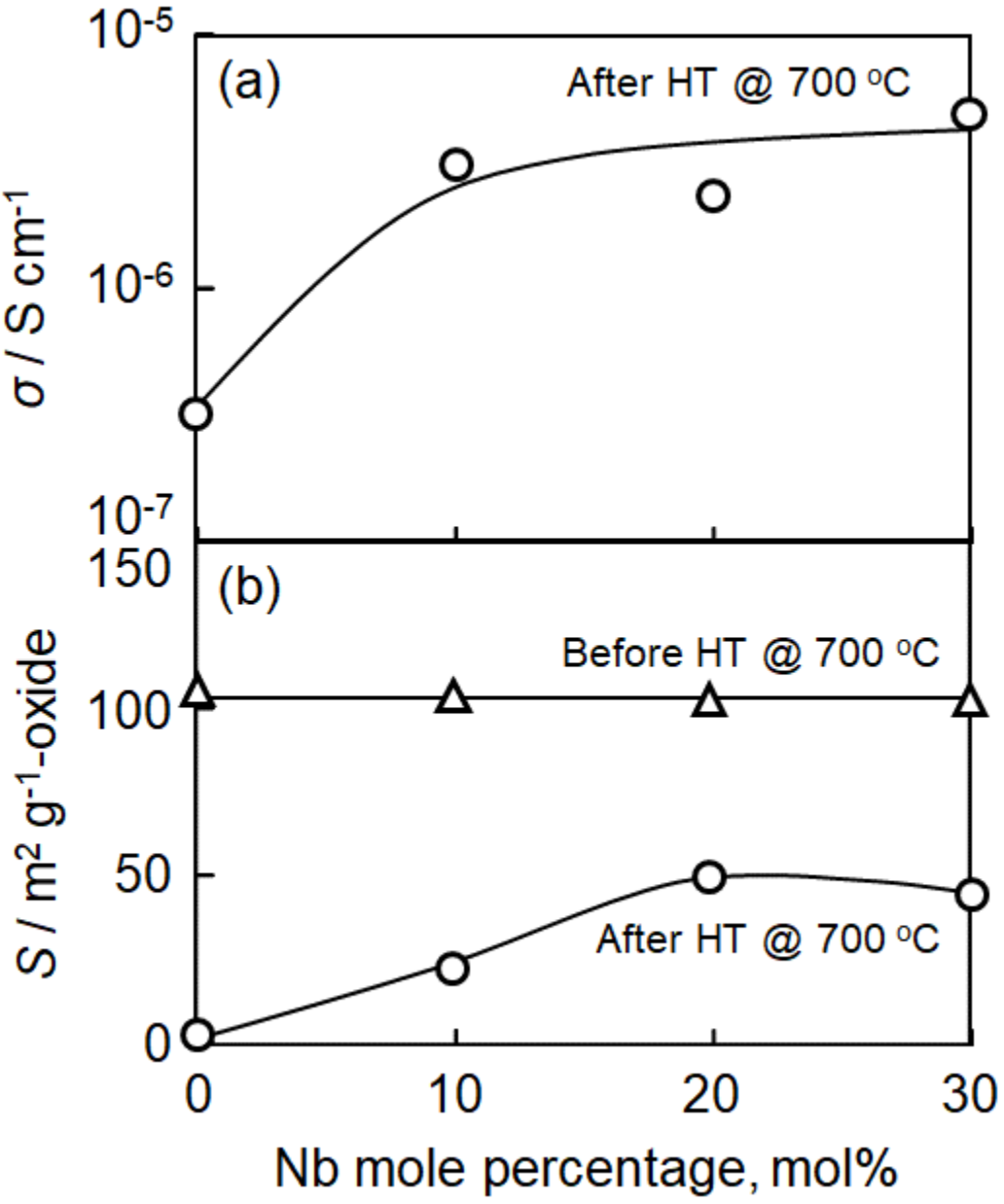

Fig. 2 Dependence of (a) the conductivity after heat-treatment at 700 °C for 10 min under 4%H_2/Ar and (b) the specific surface area before and after heat-treatment at 700 °C for 10 min under 4%H_2/Ar of the titanium-niobium oxides on the Nb mole percentage.

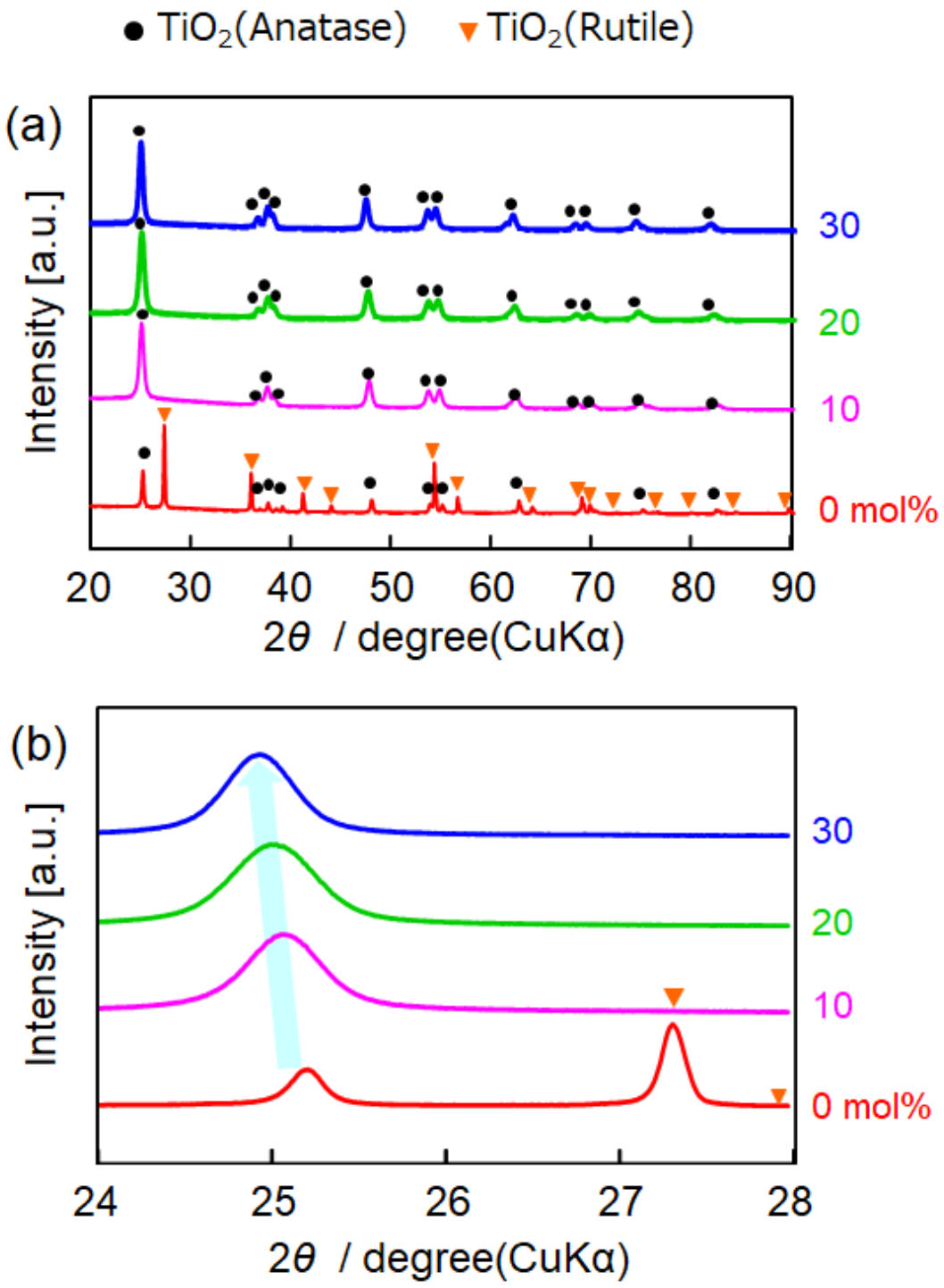

Fig. 3 XRD patterns of the catalysts with (a) a scan range of 20 – 90° and (b) a narrow range of 24 – 28°.

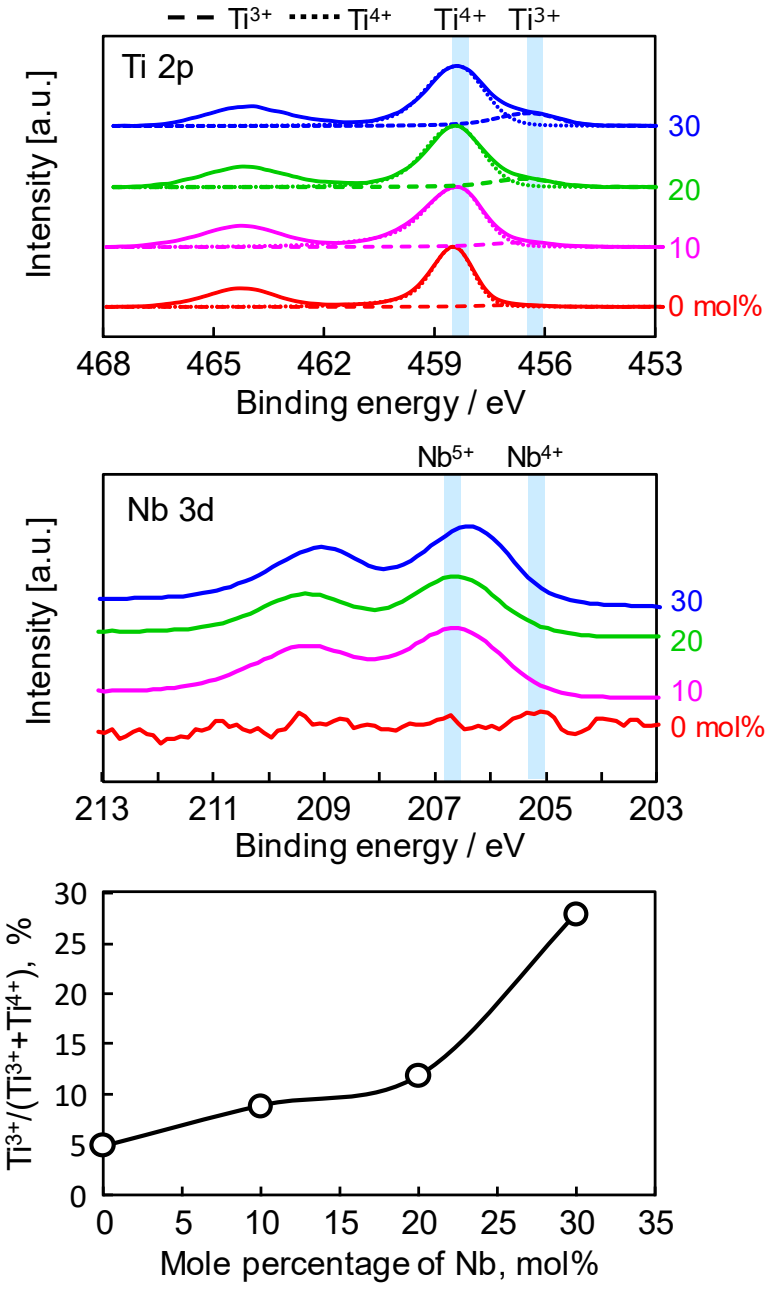

Fig. 4 (a) Ti 2p and (b) Nb 3d XPS spectra of the Nb-TiO_2 catalysts. (c) Dependence of the ratios of $Ti^{3+}/(Ti^{4+}+Ti^{3+})$, $S_{Ti(III)}/(S_{Ti(IV)}+S_{Ti(III)})$ calculated from areas of the Ti 2p spectra of the Nb-TiO_2 catalysts on the mole percentage of Nb.

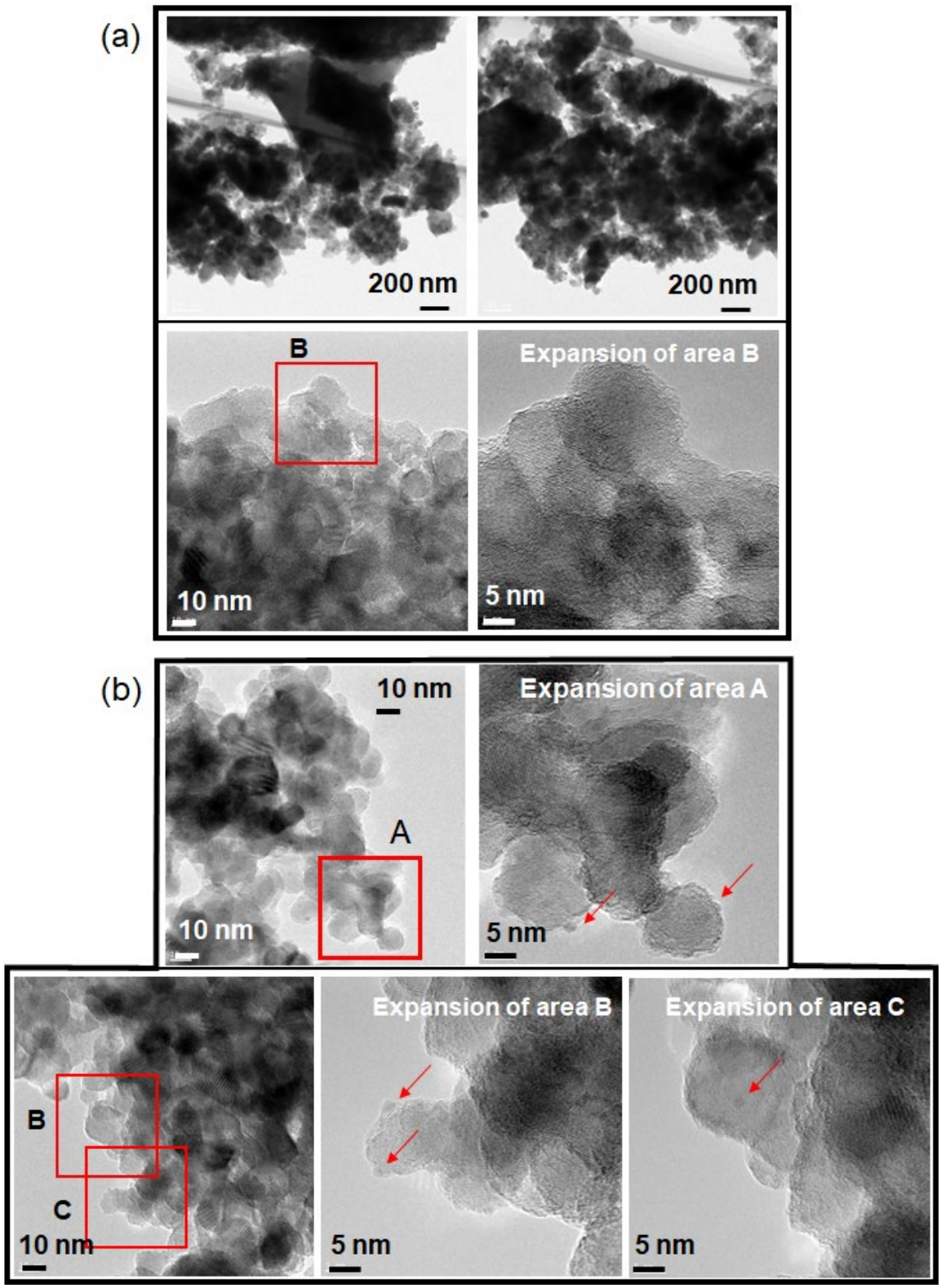
(a)
200 nm
200 nm
B
10 nm
Expansion of area B
5 nm
(b)
10 nm
A
10 nm
Expansion of area A
5 nm
B
C
10 nm
Expansion of area B
5 nm
Expansion of area C
5 nm

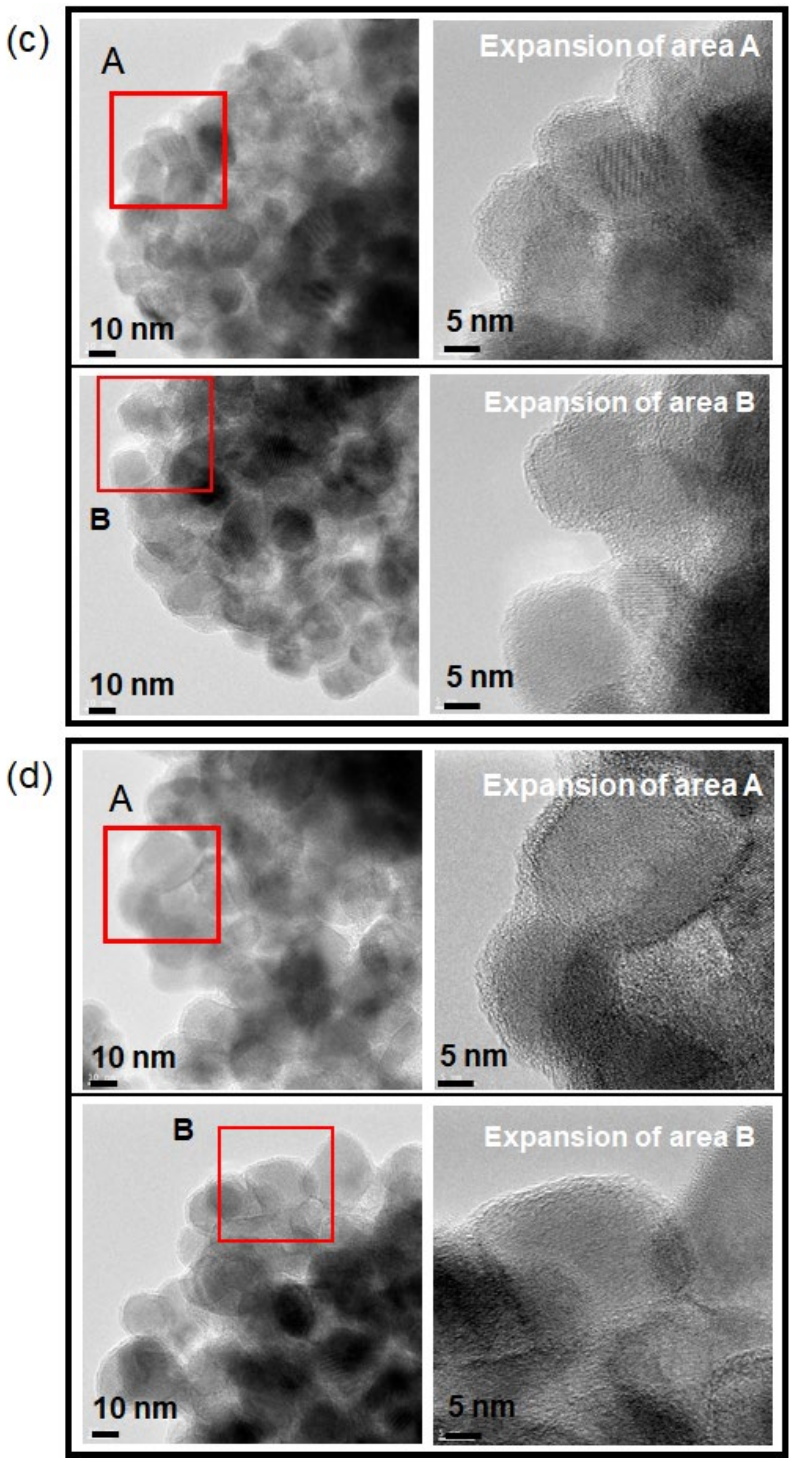

Fig. 5 TEM images of (a) 0mol%Nb-TiO_2, (b) 10mol%Nb-TiO_2, (c) 20mol%Nb-TiO_2, and (d) 30mol%Nb-TiO_2.

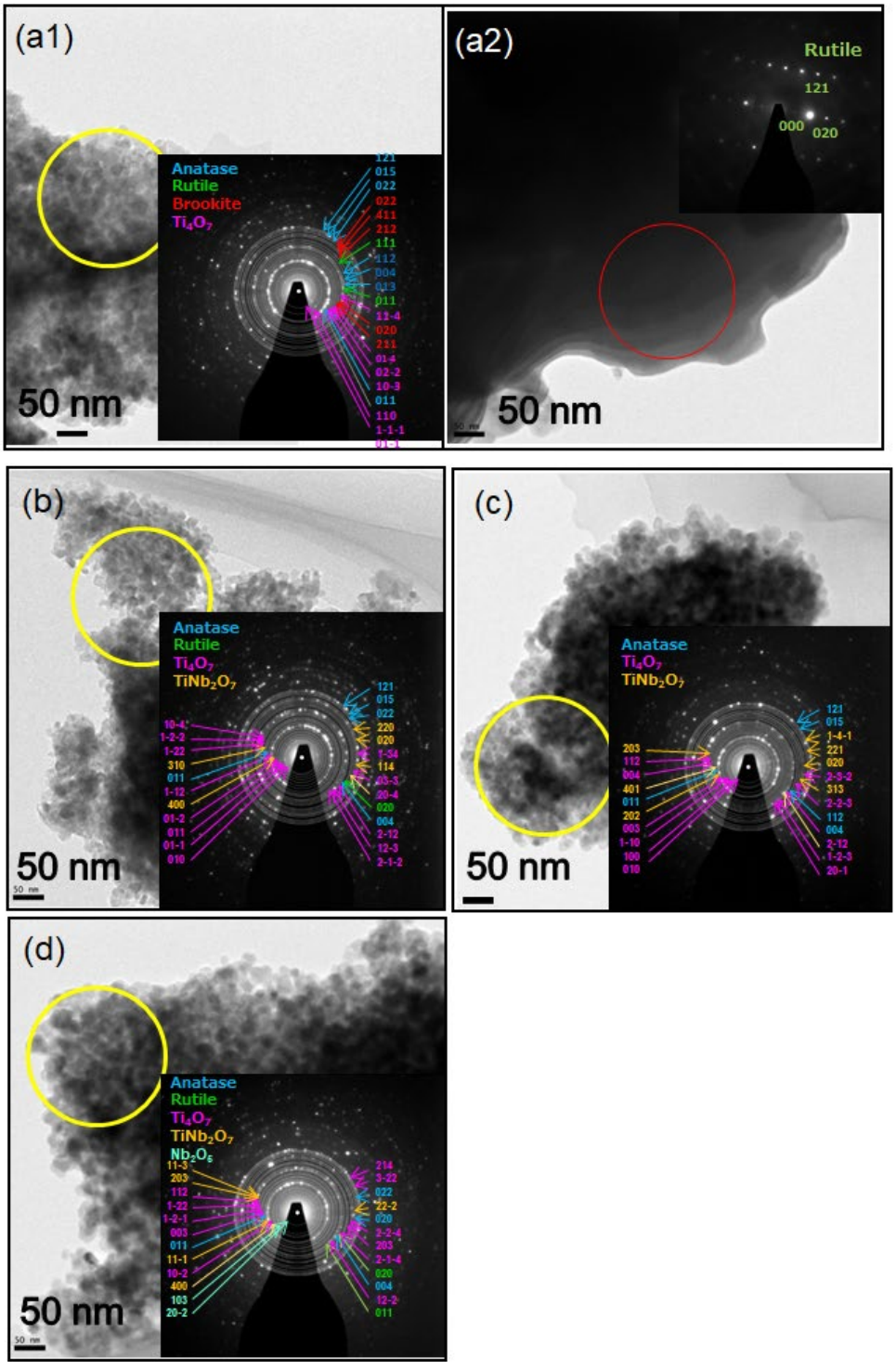

Fig. 6 TEM images and corresponding SAED of (a1) and (a2) 0mol%Nb-TiO_2, (b) 10mol%Nb-TiO_2, (c) 20mol%Nb-TiO_2, and (d) 30mol%Nb-TiO_2.

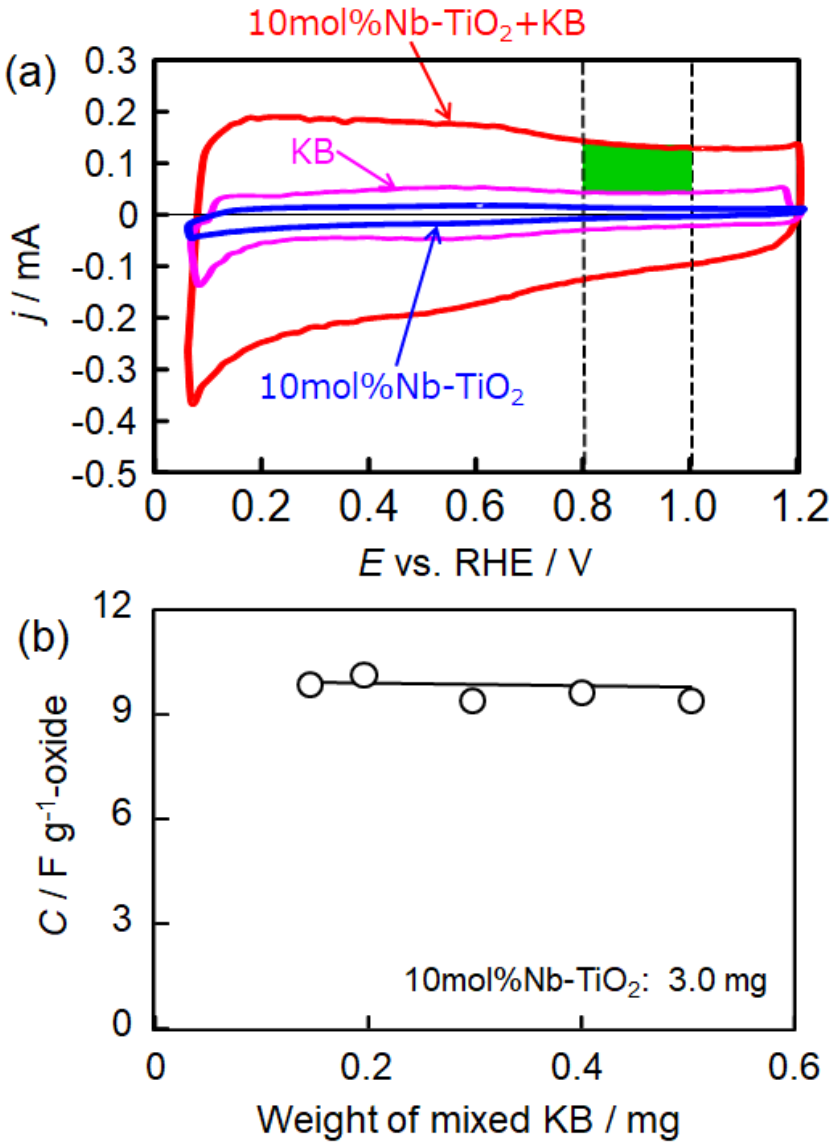

Fig. 7 (a) Cyclic voltammogram (CV) of the mixture of 10mol%Nb-TiO_2 and KB with a weight ratio of 10:1 (red line) and CV of the pure KB with equivalent weight in the mixture (pink line) and CV of the pure 10mol%Nb-TiO_2 with equivalent weight in the mixture (blue line) in 0.1 M H_2SO_4 at 30 °C under inert atmosphere. (b) Dependence of the capacitance based on the oxide mass on the weight of mixed KB when the weight of the 10mol%Nb-TiO_2 was fixed at 3.0 mg.

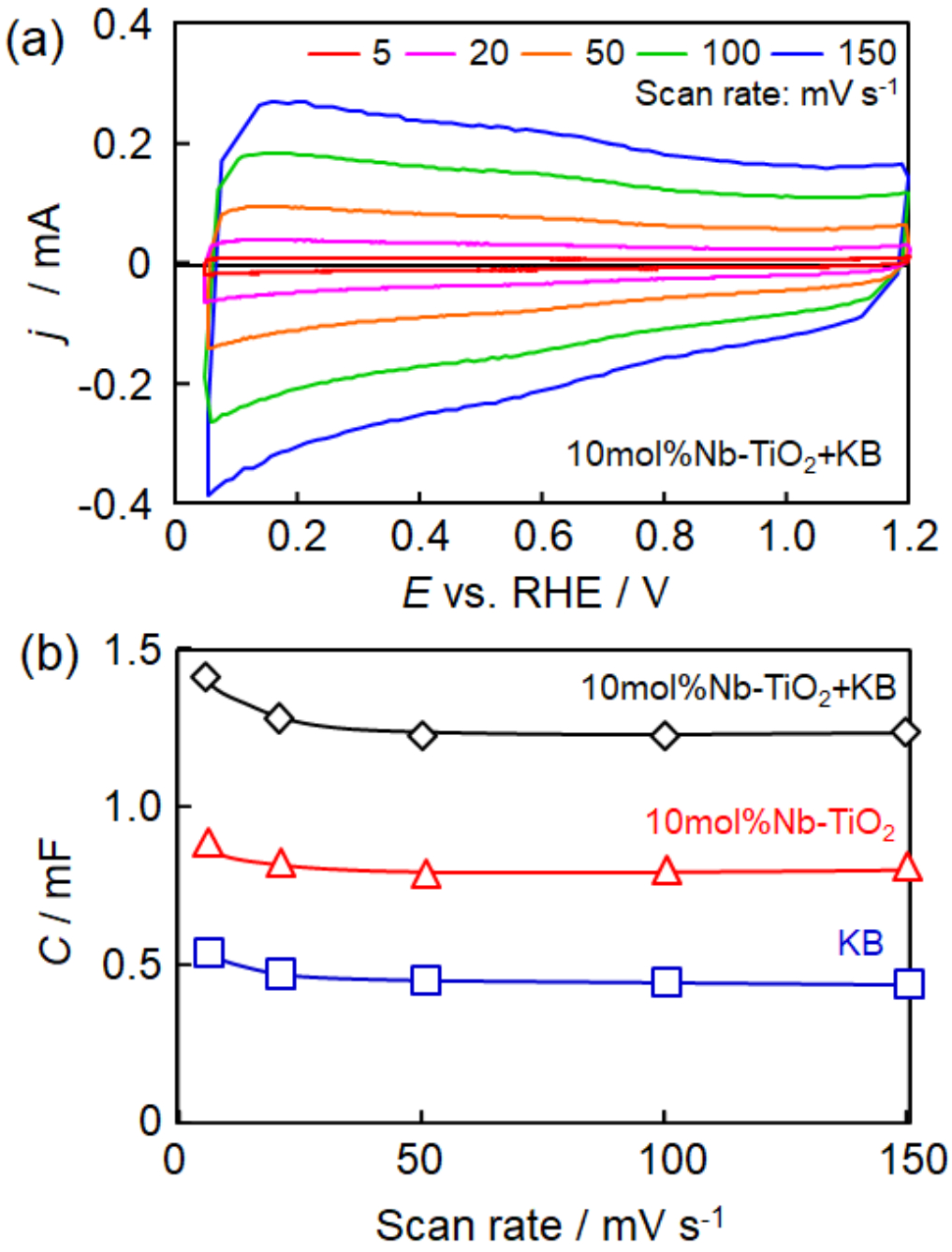

Fig. 8 (a) Effect of a potential scan rate on the CVs of the mixture of 10mol%Nb-TiO_2 and KB with a weight ratio of 10:1. (b) Dependence of the potential scan rate on the capacitance calculated from the CVs in the potential range from 0.8 to 1.0 V.

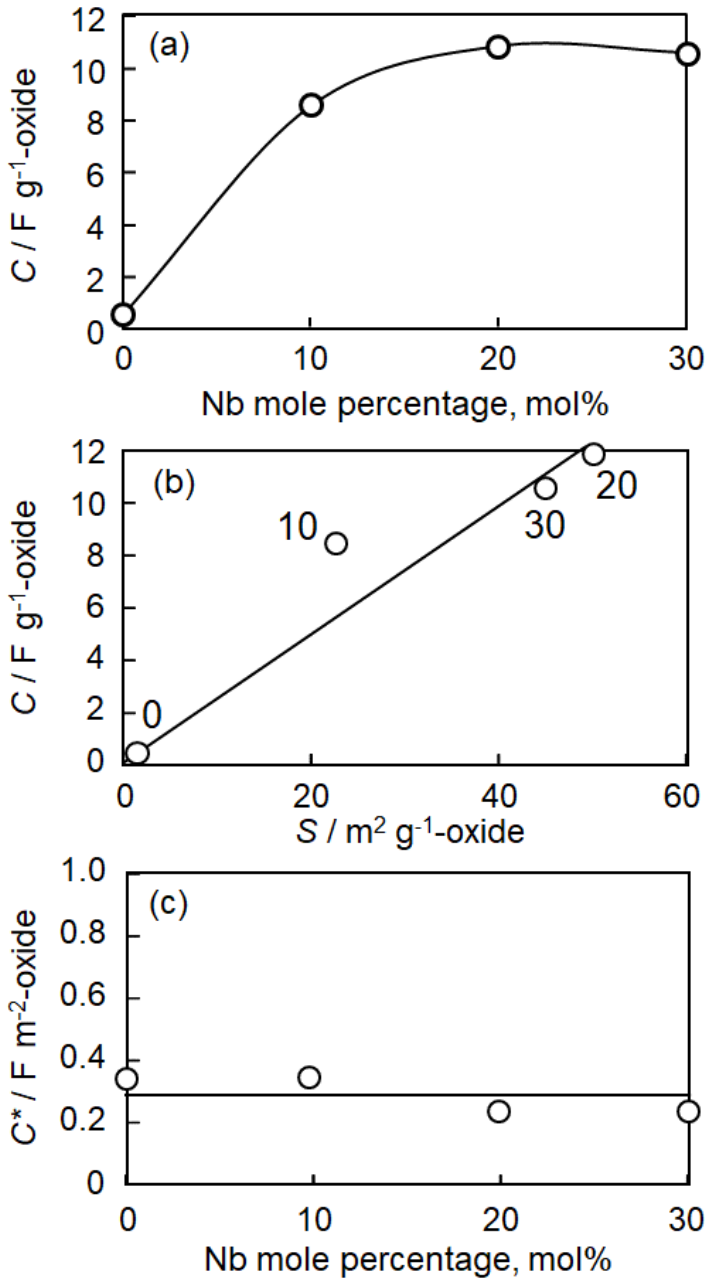

Fig. 9 (a) Dependence of the capacitance of the oxide catalysts on the Nb mole percentage, (b) Relationship between double layer capacitance based on mass of oxides and specific surface area, (c) Dependence of the capacitance based on specific surface area on the Nb mole percentage.

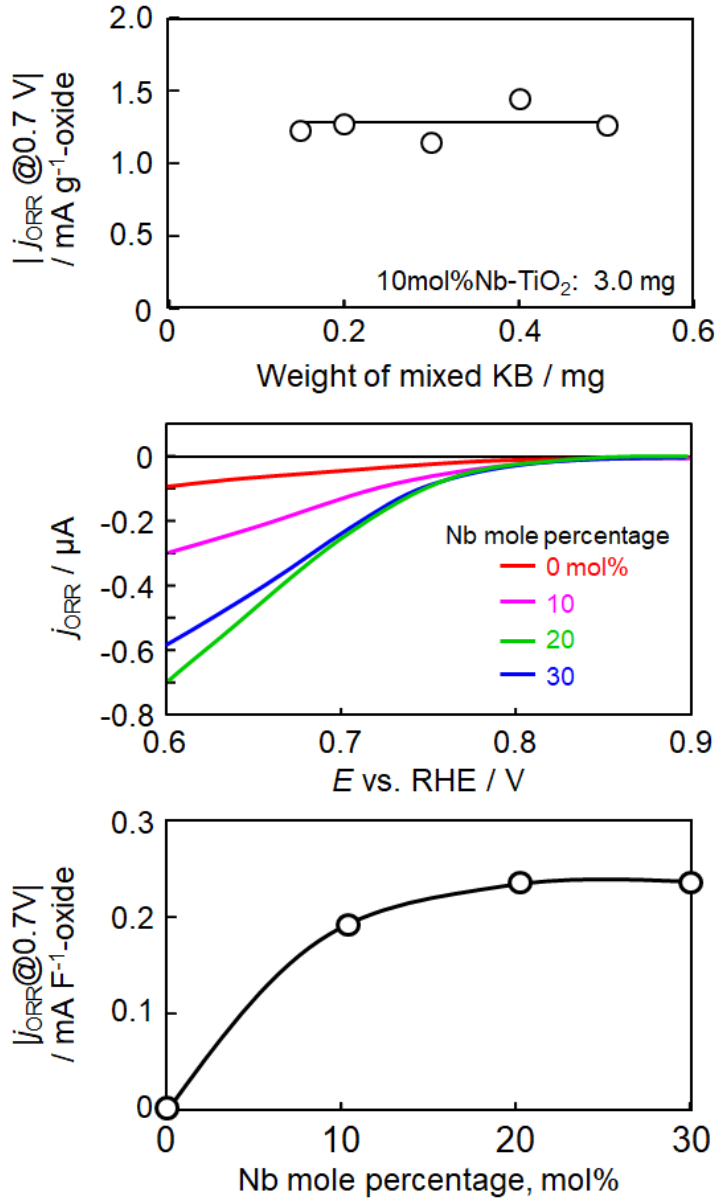

Fig. 10(a) Dependence of the ORR current density based on the mass of the 10mol%Nb-TiO_2 on the weight of mixed KB when the weight of the 10mol%Nb-TiO_2 was fixed at 3.0 mg, (b) Potential-ORR current curves for the ORR of the mixture of KB and catalysts, and (c) Dependence of the ORR current density at 0.7 V based on the capacitance of the Nb-TiO_2, |j_{ORR}@0.7V|, on the Nb mole percentage in 0.1 M H_2SO_4 at 30 °C.

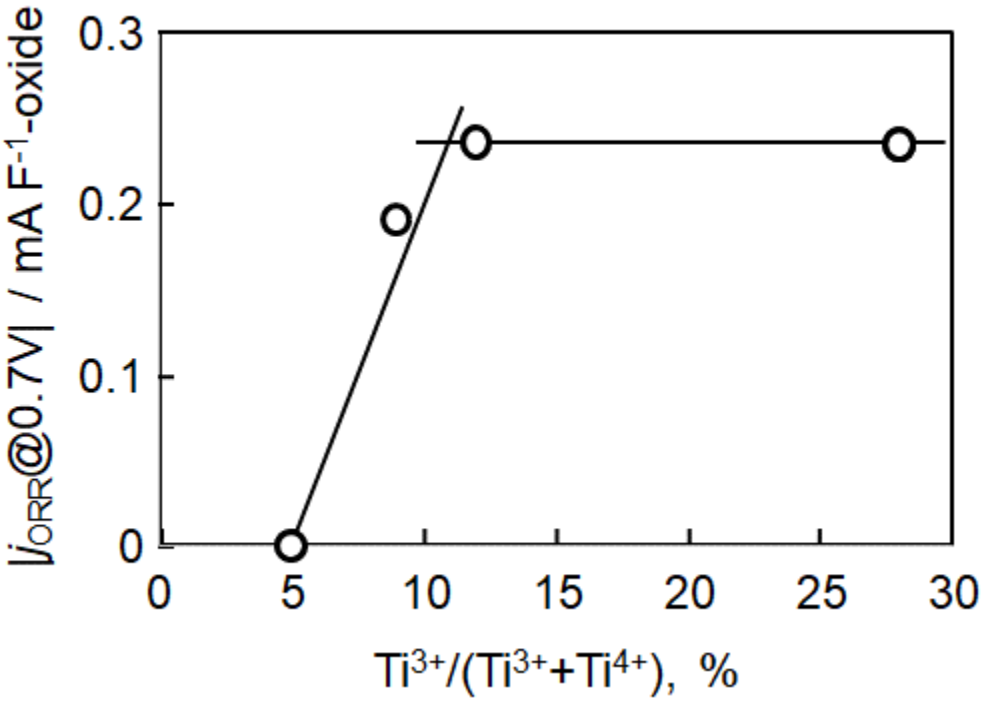

Fig. 11 Relationship between the $|j_{ORR}@0.7V|$ and the ratio of $Ti^{3+}/(Ti^{4+}+Ti^{3+})$.

Table 1 Ti-element mole ratio of element to Ti, the content with a unit of mol%, and the atomic ratios of Nb/(Ti+Nb) near the surface of each sample.

Nb mole %		Ti (2p)	Nb (3d)	O (1s)	C (1s)	Nb/(Nb+Ti), %
0	Mole ratio against Ti	1		2.4	0.92	0
	content %	23		56	21	
10	Mole ratio against Ti	1	0.17	2.7	0.41	15
	content %	23	4.1	63	9.5	
20	Mole ratio against Ti	1	0.39	3.5	1.1	28
	content %	16	6.4	58	19	
30	Mole ratio against Ti	1	0.75	5	1.1	43
	content %	13	9.5	64	14	